JOURNAL OF PROPULSION AND POWER
Vol. 23, No. 3, May–June 2007

# Effect of Ambient Gas Density on Spray Characteristics of Swirling Liquid Sheets

Dongjun Kim,* Ji-Hyuk Im,† Hyeonseok Koh,‡ and Youngbin Yoon§
*Seoul National University, Seoul 151-742, Republic of Korea*

DOI: 10.2514/1.20161

**The spray and breakup characteristics of a swirling liquid sheet were investigated by measuring the spray angle and breakup length as the axial Weber number $We_l$ was increased up to 1554 and the ambient gas pressure up to 4.0 MPa. As the $We_l$ and ambient gas density $\rho$ increased, the disturbances on the annular liquid sheet surface were amplified by the increase of the aerodynamic forces, and thus the liquid sheet disintegrated from the injector exit. The measured spray angles according to the ambient gas density differed before and after the sheet broke up. Before the liquid sheet broke up, the spray angle was almost constant; however, once the liquid sheet started to break up, the spray angle decreased. As the ambient gas density and $We_l$ increased, the increasing aerodynamic force caused the breakup length to decrease. Finally, the measured breakup lengths according to the ambient gas density and $We_l$ were compared with the results of the linear instability theory. Considering the attenuation of sheet thickness in the linear instability theory, the corrected breakup length relation agreed well with our experimental results.**

## Nomenclature

| | | |
|---|---|---|
| $C_d$ | = | discharge coefficient |
| $h$ | = | annular sheet thickness at $(r, x)$ |
| $h_0$ | = | initial sheet thickness at injector exit |
| $i$ | = | number of tangential inlet |
| $K$ | = | injector constant, $Rr_0/ir_p^2$ |
| $K_\lambda$ | = | equivalent injector constant |
| $\dot{m}$ | = | spray mass flow rate |
| $P_c$ | = | ambient gas pressure |
| $R$ | = | swirl arm from axis of injector to center of tangential inlet |
| $Re$ | = | Reynolds number |
| $r_p$ | = | tangential inlet radius |
| $r_0$ | = | orifice radius |
| $u$ | = | axial velocity |
| $We_g$ | = | gas Weber number based on gas density, $\rho_g u^2 h_0/\sigma$ |
| $We_l$ | = | axial Weber number, $\rho_l u^2 h_0/\sigma$ |
| $w$ | = | tangential velocity |
| $z$ | = | axial distance from the injector exit |
| $z_b$ | = | sheet breakup length |
| $\beta$ | = | growth rate of wave |
| $\Delta P$ | = | injection pressure difference |
| $\eta_b$ | = | amplitude of wave at breakup |
| $\eta_i$ | = | initial amplitude of wave at the injector exit |
| $\theta$ | = | spray half-angle |
| $\theta_0$ | = | equivalent spray half-angle |
| $\lambda$ | = | friction coefficient |
| $\rho_g$ | = | ambient gas density |
| $\rho_l$ | = | liquid density |
| $\sigma$ | = | surface tension |

Received 21 September 2005; revision received 2 November 2006; accepted for publication 6 December 2006. 

*Ph.D. Candidate, School of Mechanical and Aerospace Engineering; kan31@snu.ac.kr.

†Ph.D. Candidate, School of Mechanical and Aerospace Engineering; noname01@snu.ac.kr.

‡Ph.D., School of Mechanical and Aerospace Engineering; aroma@snu.ac.kr.

§Professor, Institute of Advanced Aerospace Technology, School of Mechanical and Aerospace Engineering, San 56-1, Shillim-dong, Gwanak-gu; ybyoon@snu.ac.kr.

## I. Introduction

THE airblast atomizer was universally accepted for aeroengine applications in the 1970s because of the innate tendency of a swirl injector to form a considerable amount of soot at high combustion pressures [1]. However, the airblast atomizer soon showed the practical disadvantages of narrow stability limits and poor atomization quality at startup, due to the low air velocity. These problems can be solved by combining the pressure-swirl injector with an airblast atomizer. The swirl injectors have many advantages such as good atomization, low combustion instability, and wide operating range because of its hydraulic spray characteristics and thus, it has been widely used in rocket engines, air-breathing engines, and industrial drying processes [2]. The circumferential flow in a swirl chamber can be generated by using a screw or a set of tangential inlets. As the circumferential flow approaches the discharge orifice, the converging part from a vortex chamber to orifice accelerates it. Because of this high tangential flow velocity, a gas core is formed around the centerline inside the injector to balance the static pressure of the working fluid and the ambient pressure. At the injector exit, the liquid is injected at a specific spray angle, whose tangent corresponds to the ratio of the axial and tangential velocities. Further downstream from the injector exit, the injected liquid becomes thin and disintegrates into droplets by hydrodynamic instability. In general, the discharge coefficient of a swirl injector is low while the spray cone angle is high.

Many studies have been conducted to reveal the basic mechanism of discharge and atomization of swirling flows and to establish the relationship among injector performances, operating conditions, and geometric parameters. Despite the extensive experimental and analytic studies, absolute correlations have yet to be established. Taylor [3] provided a theoretical treatment by considering the swirling flow as a potential flow and suggested that the film thickness is linearly related to the spray cone angle. Bayvel and Orzechowski [4] summarized that by assuming inviscid flow, the spray characteristics, such as discharge coefficient, spray cone angle, and film thickness, are a function of a single injector dimension defined as the injector constant, $K = Rr_0/ir_p^2$. Here, $R$ is the swirl arm from the axis of the injector to the center of the tangential inlet, $r_0$ and $r_p$ are the radii of the orifice and tangential inlet, respectively, and $i$ is the number of tangential inlets. Rizk and Lefebvre [5] performed a systematic theoretical and experimental study on the internal and external flow characteristics in the swirl injector. They derived that the spray cone angle and film thickness were functions of the injector dimensions and liquid properties, assuming that only pressure and viscous forces acted on the liquid flow inside the orifice.

Although the effects of the injection conditions and geometries on spray angle and breakup length have been widely investigated for several decades, the experiments have been confined to atmospheric conditions. In practical applications, the combustion of a liquid rocket, gas turbine, or diesel engines using swirl injectors occurs at a very high pressure, and it has been reported that the spray characteristics at high pressure conditions were much different from those at atmospheric conditions. Much of the work in the early 1990s on the effects of elevated ambient density on the spray characteristics were performed with diesel injectors at very high injection pressures. De Corso and Kemeny [6] investigated the effects of injection and ambient pressures on the spray angle of swirl injectors and found that the spray angle is inversely proportional to $\Delta P \rho^{1.6}$. The swirl injectors of liquid rocket or gas turbine engines using relatively low injection pressure have been studied since the mid-1980s; however, most of these studies were concentrated on the atomization quality of the swirl injector [7–9]. A representative study by Wang and Lefebvre [7] measured the mean drop size and drop size distribution over wide ranges of liquid properties and ambient gas pressures. They concluded that the basic effect of increased gas pressure is the improvement in atomization, but the contraction of the spray angle by the increased gas pressure reduces the relative velocity between the droplets and the surrounding gas and also increases the possibility of drop coalescence. Hence, a continuous increase in gas pressure caused the Sauter mean diameter (SMD) to first increase up to a maximum value and then decline.

In this study, the effect of ambient gas density on the spray shape and breakup characteristics of a swirl injector was investigated by measuring the spray angle and breakup length. Because the breakup of a swirl spray is mainly controlled by the aerodynamic forces between the liquid sheet and ambient gas, the axial Weber number $We_l$ (or sheet velocity) is also considered as an experimental variable. The main objective of the present study is to understand the spray patterns and the breakup phenomenon, which have an important influence on the atomization process at high ambient pressures and relatively low injection pressures of a swirl injector. In addition, the measured breakup lengths of the swirling annular sheets were compared with the linear instability theory, which can describe the disintegration of liquid sheets.

## II. Experimental Methods

### A. Experimental Conditions

The swirl injector, used in the experiments, was designed according to the hydraulics of Bayvel and Orzechowski [4] as shown in Fig. 1. The orifice diameter $d_0$ was 2 mm and the tangential inlet had three holes with the diameter $d_p$ of 1 mm at every 120 deg. The injector was designed as a closed type consisting of a separate vortex chamber and orifice: the contraction ratio of the vortex chamber to the orifice diameter was set to 3. Table 1 shows the experimental conditions and parameters. The injection pressure differential was varied from 0.061 to 0.579 MPa, which corresponds to the mass flow rate range of 8.73 to 25.51 g/s, respectively. The axial Weber number $We_l$, defined as $\rho_l u^2 h_0/\sigma$, was calculated using Eqs. (3) and (4), according to the injection pressure as shown in Table 1, and the experimental results are expressed in $We_l$, hereafter.

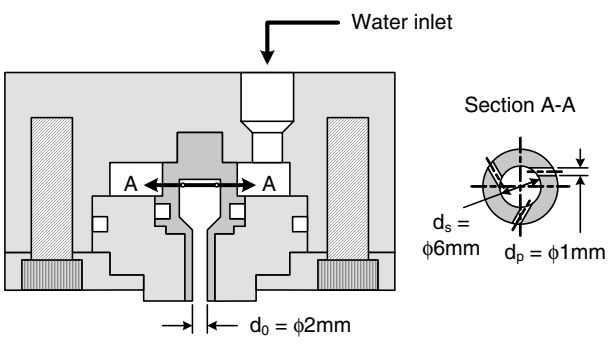


**Fig. 1 Swirl injector design.**

**Table 1 Experimental conditions and parameters**

| *Injection conditions (stimulant: water)* | |
|---|---|
| Injection pressure, MPa | Axial Weber no. $We_l$ |
| 0.061 | 170 |
| 0.133 | 365 |
| 0.207 | 564 |
| 0.281 | 762 |
| 0.355 | 960 |
| 0.429 | 1157 |
| 0.504 | 1356 |
| 0.579 | 1557 |
| *Ambient conditions (pressurizing gas: nitrogen)* | |
| Ambient gas pressure, MPa | Density ratio $\rho_g/\rho_l(\times 10^{-3})$ |
| 0.1 | 1.12 |
| 0.2 | 2.25 |
| 0.5 | 5.62 |
| 1.0 | 11.24 |
| 2.0 | 22.49 |
| 4.0 | 44.98 |

To investigate the effect of ambient gas pressure and injection velocity on the spray characteristics, the high pressure chamber system was used. The high pressure system includes four parts: a main chamber, propellants supply tanks, gas supply tanks, and a controller. The endurance pressure of the main chamber was designed to 12 MPa, but the nitrogen gas was pressurized into the main chamber up to 4 MPa for safety. The diameter and volume of the main chamber was 500 mm and 200 l, respectively. For position variation in pressurized conditions, the injector was able to vertically transverse by a device on the main chamber cover. Because the pressure of the main chamber increases when the spray is injected, the increased pressure needs to be reduced to maintain the designed chamber pressure; the controller automatically determines this process by sensing the chamber pressure and then opening and closing the exhaust valve. In addition, the injection pressure slowly decreases because the gas volume increases in the water supply tank as the water is injected, and thus the controller supplements the pressure in the similar method. The gas-curtain systems were set on four windows to reduce the deposition of droplets on the inner window surfaces. The pressure increment by the injection of the gas curtain is also exhausted by the controller.

### B. Experimental Techniques

The spray cone angle and breakup length were measured using instantaneous spray images taken by indirect photography. The stroboscopic light with a luminous time of less than 4 $\mu$s was illuminated through a translucent paper. The exposure time of a charge-coupled device (CCD) camera (KODAK ES1.0, 1008× 1008) was set to be identical to the flash interval of the stroboscope to take one image per flash without extra synchronization. Sixty images were taken for one experimental case, and the deviations of data were less than 10% from their mean values.

For the quantitative measurement of laser diagnostics in an optically dense spray, the intensity of the attenuated signal should be corrected. Therefore, the optical line patternator [10] was applied to obtain the original distribution of the dense spray under a high ambient pressure environment. The optical line patternator is a combined technique of the laser extinction measurement and image processing for the spray characterization. The spray was scanned with the laser beam (He–Ne laser) and the transmission intensity through the spray was detected by a photodiode, as shown in Fig. 2a. The line image of Mie scattering was captured simultaneously in the path of each laser beam by using a CCD camera. The distribution of the attenuation coefficients in the spray was obtained by processing the distribution data of transmission intensity $I_{n,j}$ and Mie-scattering intensity $G_{i,1}$ by an algebraic reconstruction technique, as shown in Fig. 2b. From the distributions of attenuation coefficients, an accurate surface distribution from the Mie-scattering signal can be obtained. The optical line patternator uses a laser beam instead of a

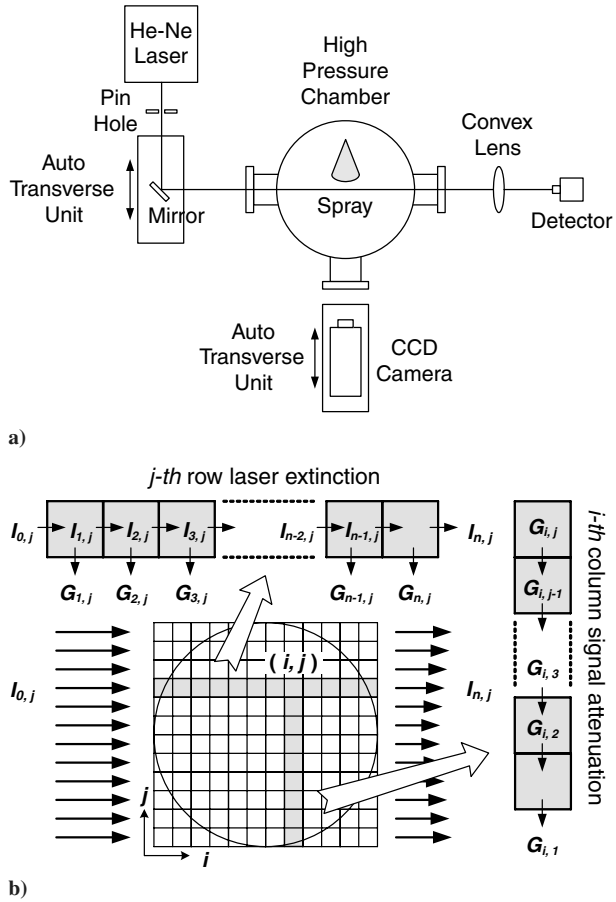


**Fig. 2 Optical line patternator; a) schematics of optical line patternator with high pressure chamber; b) principle of algebraic reconstruction of measured plane.**

laser sheet to scan the spray, and thus the effect of multiple scattering due to the increased number density of droplets in a high pressure environment can be reduced significantly.

## III. Results and Discussion

The initial liquid film properties at the orifice exit, such as film thickness $h_0$, axial velocity $u_0$, and tangential velocity $w_0$, are required to predict the shape and spray angle of the annular liquid sheet. These properties also greatly affect the shape and spray angle. By assuming that the internal flow of a swirl injector is inviscid, the tangential velocity at the orifice exit can be easily determined by the angular momentum conservation. The internal flow characteristics are a function of only the injector constant, $K = Rr_0/ir_p^2$. These internal flow characteristics including the effect of viscosity on the operation of the swirl injector have yet to be fully interpreted. The friction forces developed at the wall of the swirl chamber due to viscosity decrease the angular momentum of a swirling flow. As a result, the angular momentum of the swirling flow in the discharge orifice should be smaller than that at the tangential inlet, and therefore, both the radius of the gas core and the spray cone angle decrease while the discharge coefficient increases [4].

Horvay and Leuckel [11] have measured the velocity fields inside the enlarged swirl injectors for a wide range of the flow Reynolds number as well as the swirl intensity parameters using the laser Doppler anemometry (LDA) system, and reported that the loss of angular momentum was a function of the flow Reynolds number, as shown in Eq. (1).

$$M_o/M_i = 1 - \exp(aRe^b) \qquad a = -0.1777K^{-2.413}$$
$$b = 0.2439K^{0.4025} \tag{1}$$

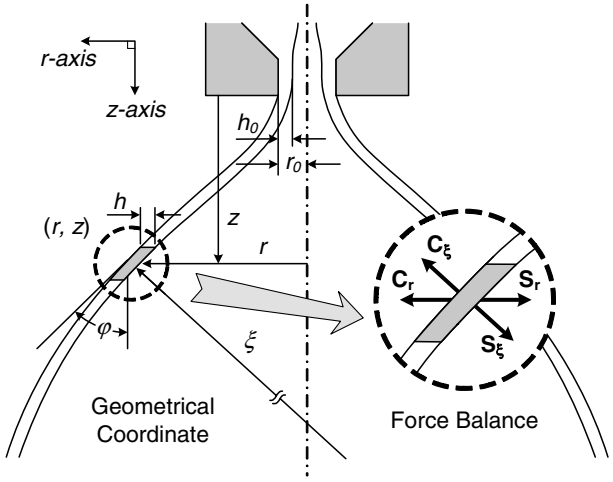


**Fig. 3 Schematic diagram of the acting forces on an annular liquid sheet.**

where $M_i$ and $M_o$ are the angular momentum fluxes at the exit of the tangential inlet and the orifice. In this study, Eq. (1) was used to calculate the tangential velocity at the orifice exit. Horvay and Leuckel [11] also found that the measured velocities of the flow at the exits of the tangential inlets are 1.3 times higher than the calculated velocities from these inlets. These higher velocities were due to the contraction of the jet by the formation of boundary layers inside the tangential inlets. Bayvel and Orzechowski [4] reported that the jet contraction ratio was varied according to the orifice shape and velocity, and suggested the experimental correlations for jet contraction ratio according to the Reynolds number. Within the present experimental conditions, the jet contraction ratios decreased slowly as the injection pressure increased and were determined to range from 0.73 to 0.65, based on the graph of Bayvel and Orzechowski [4]. Based on the determined jet contraction ratios, the initial angular momentum at the exits of the tangential inlets $M_i$ and the angular momentum at the orifice exit $M_o$ could be calculated.

### A. Spray Patterns

The shapes of the annular liquid sheets can be calculated by the force balance between liquid sheets as shown in Fig. 3. The centrifugal forces, $C_r$ and $C_\xi$, tend to cause the liquid sheet to diverge, while the surface tension forces, $S_r$ and $S_\xi$, keep the liquid sheet from diverging. Usually the gravitational force is negligible and both the inner and outer sheet surfaces encounter frictional forces, which decelerate the liquid sheet. However, the friction coefficients, which are needed for the frictional term, were neglected because they should be determined by the experiments, and unsuitable values can lead to a preposterous result. The force balance in the normal direction to the sheet surface can be derived to describe the motion of a swirling liquid sheet as in Eq. (2):

$$\frac{2\sigma}{\xi} + \frac{2\sigma}{r}\cos\varphi - \frac{\rho_l w^2 h}{r}\cos\varphi = \frac{\rho_l (u/\cos\varphi)^2 h}{\xi} \tag{2}$$

where $\xi$ is the radius of curvature, $h$ the sheet film thickness, and $\varphi$ is the tangent angle at the position of $(r, z)$. Neglecting aerodynamic drag and viscous losses, the tangential velocity $w$ at the position $(r, z)$ could be expressed as a function of $r$ by conservation of angular momentum, $wr = w_0 r_0$. Here, the initial tangential velocity at the orifice exit $w_0$ was calculated from Eq. (1) by Horvay and Leuckel [11]. The axial velocity $u$ at the position $(r, z)$ was assumed to be a constant and identical to the axial velocity at the orifice exit $u_0$, determined by the mass flow rate as shown in Eq. (3):

$$\dot{m} = \rho_l u_0 A_l = \rho_l u_0 \pi h_0 (2r_0 - h_0) \cong 2\pi\rho_l u_0 r_0 h_0 \tag{3}$$

where $A_l$ is the flowing area and $h_0$ is the film thickness at the orifice exit. Therefore, the determination of $h_0$ is crucial in the calculation of

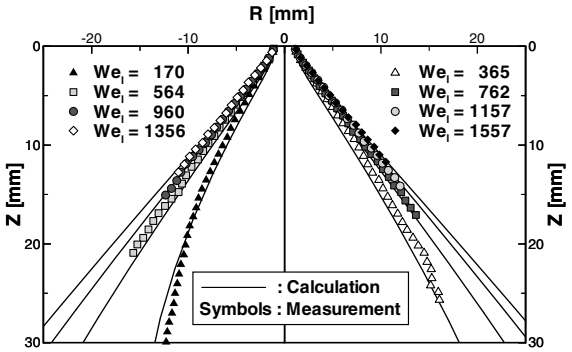


**Fig. 4 Comparison of the shapes of the annular liquid sheets according to the axial Weber number $We_l$ between the calculation (lines) and measurement (symbols).**

the flow properties at the orifice exit including $u_0$. In the present study, Eq. (4) by Bayvel and Orzechowski [4], which considers the pressure distribution at the orifice, was used to calculate $h_0$:

$$C_d = \sqrt{1 - C_d^2 K^2} - S\sqrt{S^2 - C_d^2 K^2} - C_d^2 K^2 \ell_n \frac{1 + \sqrt{1 - C_d^2 K^2}}{S + \sqrt{S^2 - C_d^2 K^2}} \tag{4}$$

where $S = (r_0 - h_0)/r_0$ is the dimensionless radius of the gas core in the discharge cross section. The discharge coefficient $C_d$ was derived from the present experimental results and the equivalent injector constant $K_\lambda$ was substituted for the injector constant $K$ (Appendix A). Finally, the liquid film thickness $h$ could be expressed as a function of $r$ by the conservation of mass flow rate as shown in Eq. (3) and the spray angle $\varphi$ could be determined by the ratio of tangential velocity $w$ to axial velocity $u$. Because all unknown variables could be expressed as a function of $r$, the shapes of the annular liquid sheets can be calculated.

The calculated shapes of the swirling liquid sheets are compared with experimental measurements in Fig. 4. Because any wave disturbances and breakup models were not considered, the predicted shapes showed a smooth and stationary curve. The symbols indicate the real spray contours according to the injection conditions, $We_l$. These contours were obtained by the image processing of the averaged images, and the experimental data were truncated when the breakup length was reached. To avoid a complicated illustration, eight injection conditions were separated into left ($We_l = 170, 564, 960, 1356$) and right sides ($We_l = 365, 762, 1157, 1554$). As the $We_l$ increased, Eq. (2) successfully predicts the shapes of the annular liquid sheets from a tulip shape to a fully developed cone and agrees well with the sheet contours by measurements. However, the momentum transfer with the surrounding gas due to friction was not considered. Thus, a slight discrepancy with the measured contour was observed at lower $We_l$. Figure 4 is to confirm the accuracy of the predicted initial film properties at the orifice exit $h_0$, which will be used for quantitative analysis of the measured data.

Figure 5 shows the effects of $We_l$ (or injection condition) and $P_c$ on the swirling liquid spray patterns. As the $We_l$ increases, the spray shape undergoes a tulip stage and grows to a fully developed cone due to the increase of tangential velocity. The disturbances on the liquid sheet surface are amplified by the increase of sheet velocity, and thus the annular liquid sheet with higher $We_l$ rapidly disintegrates from the injector exit. In addition, the increased aerodynamic drag caused by the increase in ambient gas pressure reduces the breakup length of liquid sheets at the same injection condition. At higher ambient gas pressures and larger mass flow rates, the sprays were dense due to the atomized droplets. To observe the effect of ambient gas pressure, the spray distributions perpendicular to the injection direction were measured by the optical line patternator. The measurements were conducted at 30 mm from the injector exit as the ambient gas pressure was increased, and the injection condition was maintained at $We_l = 1157$. The spray distribution of the atmosphere ambient condition in Fig. 6a shows the

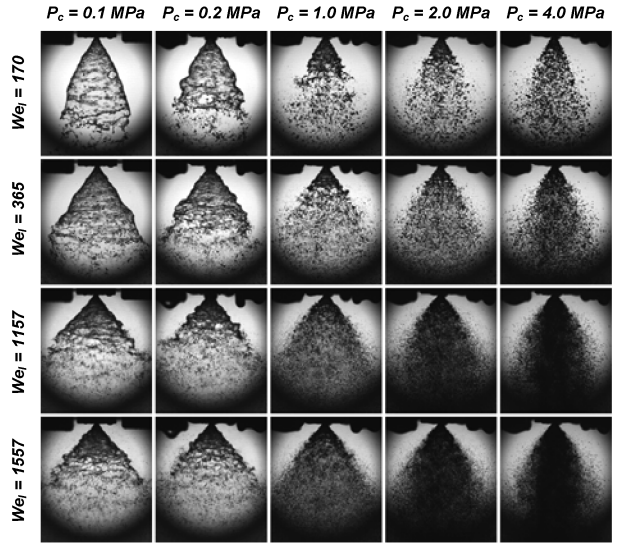


**Fig. 5 Spray patterns of the swirling liquid sheets according to the axial Weber number $We_l$ and ambient gas pressure ($We_l = 170, 365, 1157, 1557$ and $P_c = 0.1, 0.2, 1.0, 2.0, 4.0$ MPa).**

typical hollow cone shape. However, as the ambient gas pressure increased, the spray width became narrowed. The atomized small droplets penetrated into the center of the injector by the entrained ambient gas, which changed the spray shape from a wide hollow cone to a narrow solid cone.

### B. Spray Angle

The spray angle produced by a swirl injector is important in combustion systems. The spray angle characterizes the spatial distribution of droplets, and thus, it has a strong influence on the interactive characteristics of a multi-element injector, ignition performance, and cooling of the injector plate in rocket engines. In the present study, the spray angle was defined as the angle between the injection axis and the connecting line of the orifice exit and the spray edge obtained from the averaged spray images.

To express both the injection condition and ambient gas density as one parameter, a gas density based Weber number $We_g$ was used as follows:

$$We_g = \frac{\rho_g u^2 h_0}{\sigma} \tag{5}$$

where $\rho_g$ is the ambient gas density. According to the definition, $We_g$ means the ratio of aerodynamic force to surface tension force and can also be found by multiplying the ambient density ratio $\rho_g/\rho_l$ by $We_l$.

Figure 1 shows the spray angle at four axial distances (5, 10, 15, 20 mm) as a function of $We_g$. Each symbol indicates the same $We_l$; hence, Fig. 7 shows the effect of the density ratio of the ambient gas to the liquid. The onset of breakup according to each injection and ambient condition, studied in the next section, is illustrated in Fig. 7, and it was noted that the variation of the spray angle according to the ambient gas density differed before and after the sheet breakup. Before the liquid sheet broke up, the spray angle was almost constant at low $We_l$. However, as the sheet velocity increased, the sheet boundary became so unstable due to the aerodynamic force of the ambient gas that some droplets detached from the liquid surface. Hence, the measured spray angle before the sheet breakup slightly increased as increasing the ambient gas density at higher $We_l$ because of these detached droplets. In reality, the spray cone angle before breakup is expected to remain essentially constant regardless of the ambient gas density. The frictional losses at both the tangential and axial velocities were similar because both velocities were of the same order. Therefore, before the liquid sheet broke, the measured spray angle remained almost constant by the balance of centrifugal and surface tension forces between the liquid sheets [6].

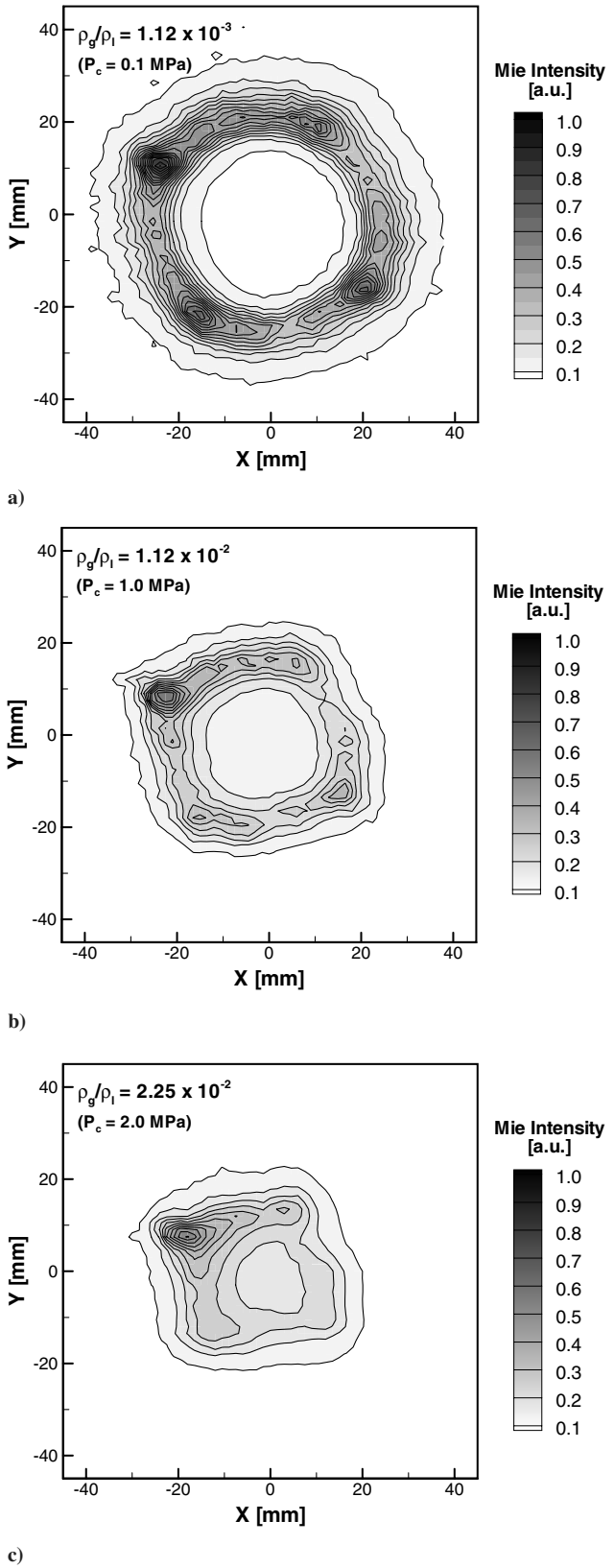


**Fig. 6 Spray distributions measured by optical line patternator with increasing ambient gas density at $We_l = 1157$: a) $\rho_g/\rho_l = 1.12 \times 10^{-3}$; b) $\rho_g/\rho_l = 1.12 \times 10^{-2}$; and c) $\rho_g/\rho_l = 2.25 \times 10^{-2}$.**

On the contrary, the spray angle after breakup was more influenced by the density ratio. Once the liquid sheet started to break up, the spray of droplets entrained ambient gas at the inner and outer surfaces of the spray. However, the inner gas volume was limited by the spray, and then the pressure difference between the inner and outer gas was produced, which caused the contraction of the spray. Lee and Tankin [12] calculated the trajectories of droplets for an annular jet and found that the small droplets were deflected from the original sheet trajectories toward the center of the spray by the entrained ambient gas. The magnitude of the gas entrainment depended on the total flow rate, the size and initial velocity of the droplets, and the ambient gas density [13]. Therefore, the contraction of the spray was more effective as increasing the ambient gas density at the same injection condition. Consequently, after the liquid sheet broke, the spray angle decreased as the ambient gas density increased because the aerodynamic effects of the entrained gas increased with increasing ambient gas density. Several publications [6,7] have reported the decrease of the spray angle with the increase of the ambient gas density; however, the degree of the reductions was different according to the measurement position.

From the results of Fig. 7, the empirical relations on the spray angle of the swirling liquid sheets were obtained as follows:

$$\text{Before breakup}: \theta/\theta_0(z) = 0.56We_l^{0.12} \tag{6}$$

$$\text{After breakup}: \theta/\theta_0(z) = 0.24We_l^{0.22}(\rho_g/\rho_l)^{-1.54We_l^{-0.56}} \tag{7}$$

To eliminate the influence of the measurement position on the spray angle, the normalized spray angle $\theta/\theta_0(z)$ was used. Here, $\theta_0(z)$ is the equivalent spray angle of a chamber pressure of 0.1 MPa and injection pressure of 0.061 MPa at each of the four axial measurement positions. Figure 8 shows the comparison between the experimental results and the above empirical relation. Because the spray angle before breakup was unaffected by the ambient gas density, it could be expressed as a function of $We_l$ alone. In contrast, the effect of $\rho_g/\rho_l$ on the spray angle after breakup was different for each $We_l$. The smaller initial spray cone angle at low $We_l$ leads to a larger pressure difference between the inner and outer gases due to the smaller enveloped volume, and consequently, the reduction of the spray angle according to $\rho_g/\rho_l$ was larger at lower $We_l$. Therefore, the index of $\rho_g/\rho_l$ on the empirical relation after breakup in Eq. (7) was expressed as a function of $We_l$. It was also observed that the measured spray angle after the breakup deviated from the empirical relation at $We_l = 170$. Because the spray at $We_l = 170$ was not a fully developed cone but tulip shaped, it could be inferred that the spray characteristics were somewhat different from other cases.

### C. Breakup Length

#### 1. *Linear Instability Theory*

Linear instability theory, which is based on the growth of waves due to the aerodynamic force on the liquid sheet surface, has been used to describe the disintegration of liquid sheets. The aerodynamic instability of the liquid sheet has been investigated on the basis of the Kelvin–Helmholtz instability [14,15]. Squire [14] was the first to investigate the instability of an inviscid liquid sheet of constant thickness. He considered two modes of disturbances: symmetric and antisymmetric modes, wherein he found that the antisymmetric mode dominated the growth of disturbances. This conclusion was later validated by extensive studies [15].

Consider a two-dimensional, inviscid, incompressible liquid sheet of thickness $2h_0$ moving with velocity $u$ through the quiescent ambient gas. The liquid and gas densities are $\rho_l$ and $\rho_g$, respectively, and the surface tension of liquid is $\sigma$. As the liquid sheet moves along the coordinate $z$, the liquid surface is disturbed. The disturbance on the liquid sheet surface is represented by $\eta$ as follows:

$$\eta = \eta_0 \exp i(kz - \beta t) \tag{8}$$

where $\eta_0$ is the initial amplitude of disturbance and $\beta$ is the growth rate. Typically $\beta$ is calculated for a spectrum for $k$. The disturbance wave number $k_{\max}$ corresponding to the maximum growth rate and $\beta_{\max}$ controls the breakup process. If the surface disturbance has reached the critical wave amplitude at breakup $\eta_b$, the breakup time

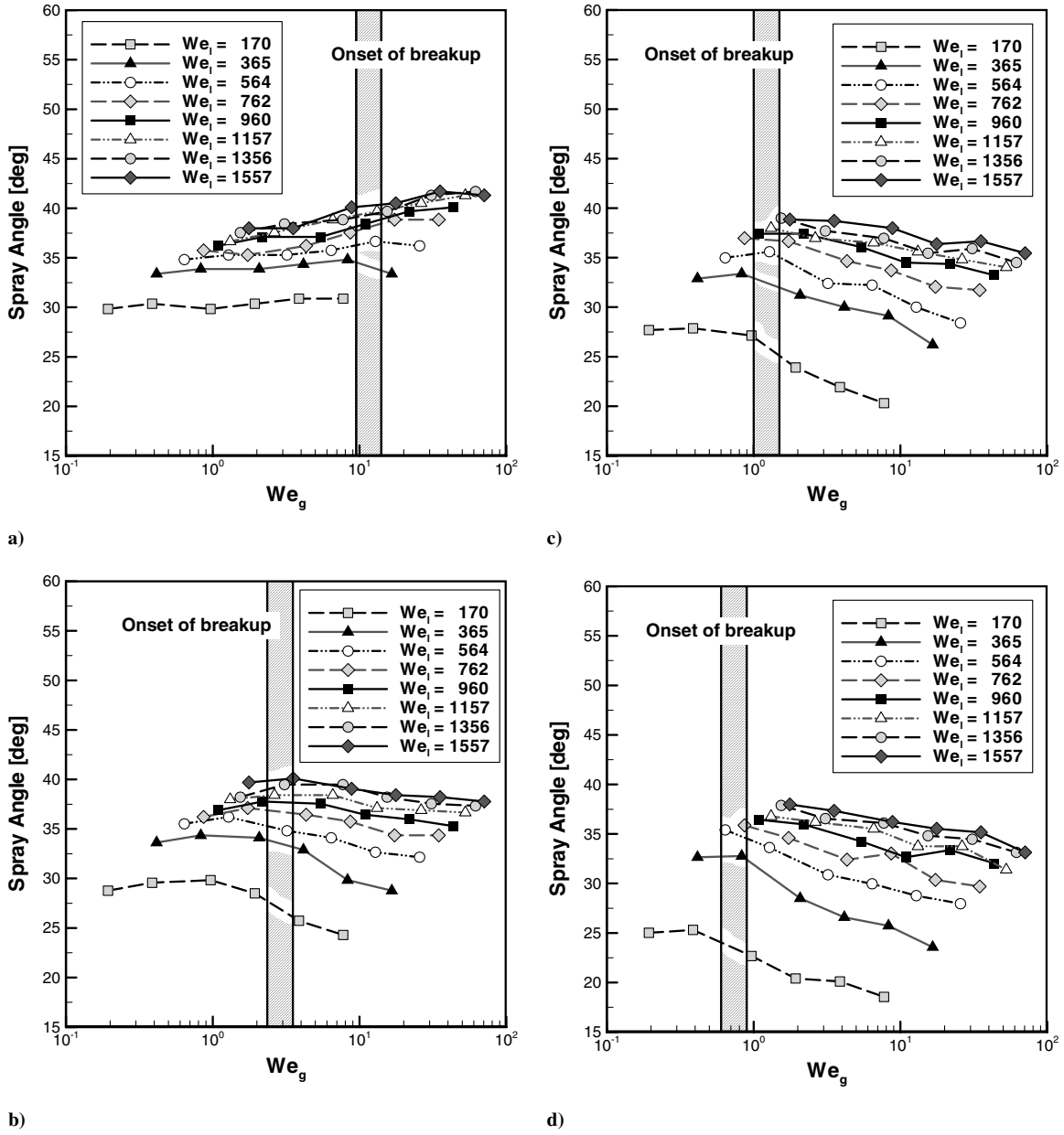


**Fig. 7 Spray angle of the swirling liquid sheets as a function of $We_g$ at the four axial distances: a) 5 mm, b) 10 mm, c) 15 mm, and d) 20 mm.**

can be calculated. The maximum growth rate is approximated as Eq. (9) and the corresponding breakup length $z_b$ can be given by Eq. (10) [15,16]:

$$\left(\frac{\beta h}{u}\right)_{\max} = \frac{1}{2}\left(\frac{\rho_g}{\rho_l}\right)\sqrt{\frac{\rho_l u^2 h}{\sigma}} = \frac{1}{2}\left(\frac{\rho_g}{\rho_l}\right) We_l^{1/2} \tag{9}$$

$$z_b = u t_b = \frac{u}{\beta_{\max}} \ell_n\left(\frac{\eta_b}{\eta_0}\right) \tag{10}$$

where $\rho_g/\rho_l$ is the density ratio of gas to liquid. Unfortunately, the theory does not predict a critical wave amplitude for sheet breakup $\eta_b$, therefore an empirical relation $\ell_n(\eta_b/\eta_0) = 12$ has been generally used [15]. However, some investigators reported that $\ell_n(\eta_b/\eta_0)$ is not a universal value and has to be determined experimentally in every case. This study was concentrated on observing the change of the breakup length according to the injection and ambient conditions. Therefore, the constant term was regarded as $C$ and the normalized breakup length relation based on the linear instability theory can be obtained as follows:

$$\frac{z_b}{h_0} = C(\rho_g/\rho_l)^{-1} We_l^{-1/2} \tag{11}$$

### 2. *Measurement of Breakup Length*

The breakup of annular liquid sheets emerging from a swirl injector undergoes a complex, unsteady, nonlinear process. The breakup begins along the length of the liquid sheet along its length in series of circular ligaments or distorted ligamentlike structures [2]. Several possible criteria for the breakup length are defined in the literature. In this study, the breakup length of a swirling liquid sheet is defined as the distance from the orifice exit where droplets are formed. The breakup length at the ambient gas pressure of 4.0 MPa cannot be measured because of the high density of spray.

The variations in the breakup length of the swirling liquid sheets according to the axial Weber number and ambient density ratio of gas to liquid are shown in Fig. 9, which also compares the linear instability theory and experimental data. The breakup lengths were normalized by the initial sheet thickness $h_0$, which was varied only with the injection condition (or $We_l$) according to Eq. (4). Figures 9a and 9b show the effects of the axial Weber number $We_l$ and the

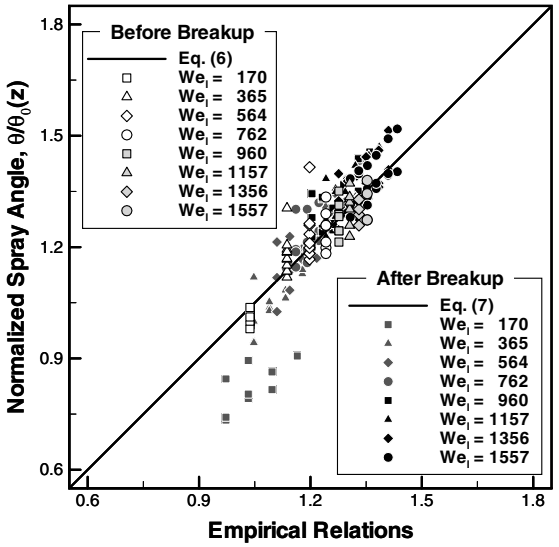


**Fig. 8 Empirical relations on the normalized spray angle $\theta/\theta_0(z)$ of the swirling liquid sheets for both cases before and after breakup.**

ambient density ratio of gas to liquid $\rho_g/\rho_l$ on the breakup lengths, respectively. As confirmed in the spray images of Fig. 5, the breakup length decreases when the aerodynamic force increases with the increase in the ambient gas density and $We_l$. The decrease of breakup length according to the increase of $We_l$ is attributed mainly to the increase of aerodynamic effects by the increase of liquid sheet velocity, and in part to the decrease in the initial liquid thickness by the increase of the injection pressure.

The difference in the breakup lengths between experiments and linear instability theory was also shown in Fig. 9. The theory itself cannot predict a critical wave amplitude for the breakup $\eta_b$, as stated above; hence, the term $\ell_n(\eta_b/\eta_0)$ in the present study is based on the work of Dombrowski and Hooper [15]. Because the critical wave amplitude for the breakup is introduced from the empirical relation of the disintegration of a planar liquid sheet, this value can be discrepant from an annular swirling liquid sheet. The linear instability theory predicts the variation of breakup length as $We_l^{-0.5}$, but the present experimental data indicate that it is proportional to $We_l^{-0.38}$. Moreover, the dependence of the normalized breakup length on the density ratio is not $(\rho_g/\rho_l)^{-1.0}$ by the linear instability theory, but rather $(\rho_g/\rho_l)^{-0.59}$. In practice, the liquid sheet, which is discharged from the injector, is attenuated as it moves away from its origin, but for simplicity, the instability theory for a sheet whose thickness remains constant has been developed. It was assumed that the main reason for the disagreement of experimental data with the linear instability theory was due to the effect of the change in the liquid sheet thickness on the sheet breakup mechanism. Dombrowski and Hooper [15] attempted to solve the breakup of the attenuated sheet; however, their assumption was different from the present swirling liquid sheet.

For a conical liquid sheet, the schematic of sheet thickness change is described as shown in Fig. 10. By assuming a mass flow rate at each perpendicular plane, the change in the sheet thickness as a function of the distance from the injector exit $z$ and the spray angle $\theta$ could be calculated. As stated in the previous section, the spray angle before breakup is independent of the ambient gas density and is only a function of $We_l$. Because $z = ut$, $h$ could be finally expressed with time as shown in Eq. (12), where $h_0$ is the film thickness at the injector exit and $r_0$ is the orifice radius:

$$h = \frac{h_0 r_0}{r_0 + z\tan\theta} = \frac{h_0 r_0}{r_0 + Ut\tan\theta} \tag{12}$$

The growth rate must be integrated over the breakup time, so that the total growth of the wave is used to predict the breakup length as in Eq. (13). As a result, the corrected linear instability theory considering the attenuation of the sheet can be obtained as shown in

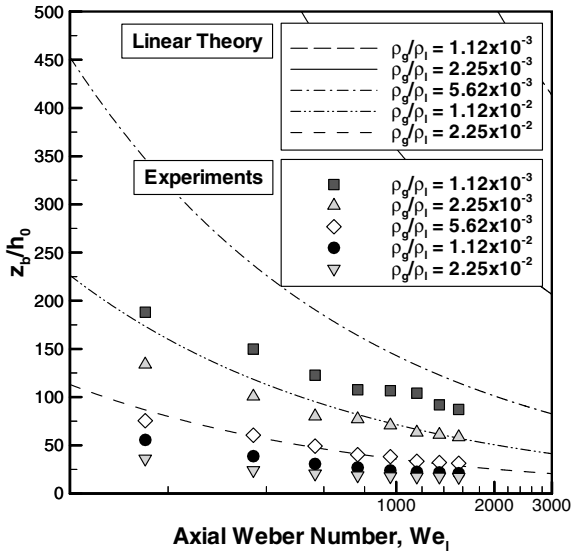


a)

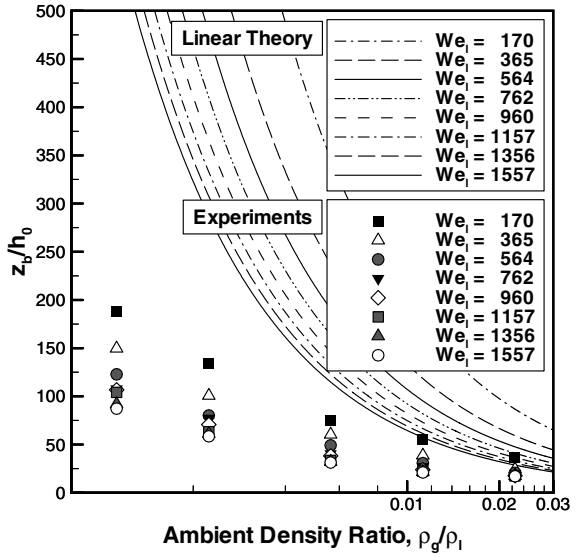


b)

**Fig. 9 Breakup length of the swirling liquid sheets according to a) axial Weber number $We_l$ and b) ambient gas density ratio of gas to liquid $\rho_g/\rho_l$.**

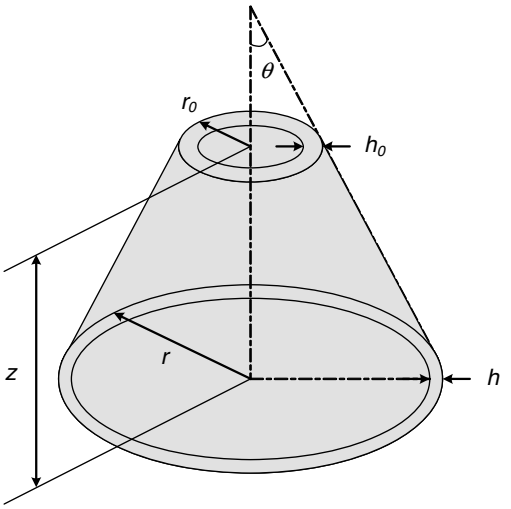


**Fig. 10 The schematics of sheet thickness change in an annular liquid sheet.**

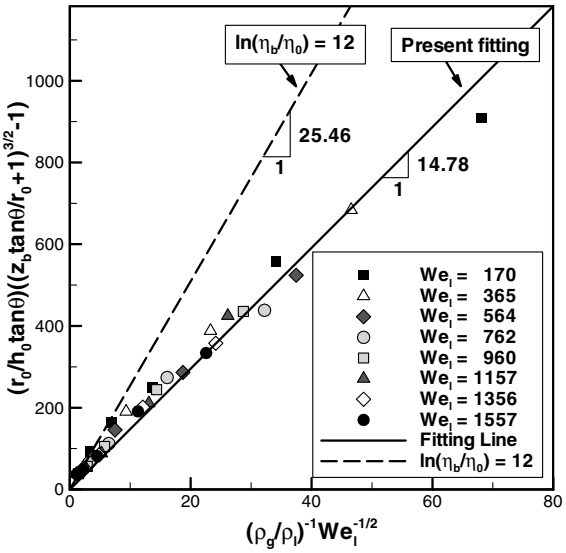


**Fig. 11 The comparison of breakup lengths between our experiment and corrected linear instability theory considering the attenuated sheet thickness.**

Eq. (14) and the developed equation is more complex (Appendix B).

$$\ell_n\left(\frac{\eta_b}{\eta_0}\right) = \int_0^{t_b} \beta_{\max}\, \mathrm{d}t \tag{13}$$

$$\left(\frac{r_0}{h_0 \tan\theta}\right)\left[\left(\frac{z_b \tan\theta}{r_0}+1\right)^{3/2}-1\right] = C(\rho_g/\rho_l)^{-1} We_l^{-1/2} \tag{14}$$

Figure 11 shows the comparison of the breakup lengths with the corrected linear instability theory considering the attenuated sheet thickness. The term of $\ell_n(\eta_b/\eta_0)$ was calculated to be about 6.9 from our experimental data, and thus the constant $C$ on the right side of Eq. (14) was determined to be 14.78. On the other hand, the dashed line in Fig. 11 was the constant value determined from the generally used empirical relation $\ell_n(\eta_b/\eta_0) = 12$. This low value of $\ell_n(\eta_b/\eta_0)$ implies that a swirling liquid sheet disintegrated quickly as compared to a liquid sheet where the liquid swirling is absent. Recent literature [17,18] has also been reported for the superior breakup performance of a swirling liquid sheet at moderate injection pressure drop. From Fig. 11, it was found that the newly developed equation predicted the breakup length of a swirling annular liquid sheet well, and the attenuation of the sheet thickness had a strong influence on the breakup mechanism of an annular swirling liquid sheet.

## IV. Conclusions

The experiments on the effects of injection conditions and ambient gas density ratio of liquid to gas on the spray shape and breakup characteristics of the swirling liquid sheets have been performed by measuring the spray angle and breakup length. To confirm the accuracy of the initial film properties at the orifice exit, the shapes of the annular liquid sheets were calculated by the force balance between liquid sheets. The calculated shapes successfully predicted the sheet contours from a tulip shape to a fully developed cone and agreed well with the measurements.

The measurement of the spray angle according to the $We_l$ and ambient gas density $\rho_g/\rho_l$ showed the different tendencies of the spray angle before and after the sheet breakup. Before the liquid sheet broke, the measured spray angle increased as the $We_l$ increased, while it remained almost constant as the ambient gas density increases. However, if the liquid sheet started to break up, the droplets entrained ambient gas and the spray angle decreased. Because of the limited volume of the inner gas, the pressure difference between the inner and outer gas was produced, which causes the contraction of the spray.

The measurements of breakup length under high ambient pressure showed that the aerodynamic force significantly affects the breakup of the swirling liquid sheets. The breakup length decreased with increasing aerodynamic force as the ambient gas density and $We_l$ increased. In addition, our experimental results on the breakup length according to the ambient gas density and $We_l$ were compared with the results using the linear instability theory. The comparison showed different dependence on the indices of each experimental variable between the two results. It was thought that this discrepancy was because the linear instability theory assumed a constant sheet thickness. Therefore, the attenuation of sheet thickness was considered in the linear instability theory, and the corrected equation agreed well with our experimental results.

## Appendix A

Borodin et al. [19] considered the effect of viscosity on a swirling flow by using the principle of the equilibrium of forces acting on a liquid element in a swirl chamber. They surmised that the decrease of the injector constant had the same effect as the decrease of the angular momentum of a swirling flow, as shown in Eq. (A1):

$$K_\lambda = \frac{K}{1+(\lambda/2)\left(R^2/ir_p^2 - K\right)} = \frac{Rr_0}{ir_p^2 + (\lambda/2)R(R-r_0)} \tag{A1}$$

Here, $K_\lambda$ is the equivalent injector constant and $\lambda$ is a friction coefficient. The relation between the friction coefficient and the Reynolds number was obtained experimentally by testing with gasoline, kerosene, and turbine oil of various injector constants and geometries [19]. Equation (A2) is the averaged curve from the experimental points:

$$\log\lambda = \frac{25.8}{(\log Re)^{2.58}} - 2, \qquad Re = \frac{u_p d}{\nu} \tag{A2}$$

where $d$ is the diameter of the equivalent inlet; hence it is given by $d = \sqrt{i}d_p$.

## Appendix B

The conical liquid sheet, discharged from the injector, is attenuated as it moves away from its origin, but for simplicity, the linear theory has not considered this effect. For a conical liquid sheet, the change of sheet thickness is given by Eq. (12) and the growth rate includes the sheet thickness as in Eq. (B1). Therefore, the growth rate has to be integrated over the breakup time $t_b$, so that the total growth of the wave is used to predict the breakup length as in Eq. (B2):

$$\left(\frac{\beta h}{u}\right)_{\max} = \frac{1}{2}\left(\frac{\rho_g}{\rho_l}\right)\sqrt{\frac{\rho_l u^2 h(t)}{\sigma}} = \frac{1}{2}\left(\frac{\rho_g}{\rho_l}\right)\sqrt{\frac{\rho_l u^2}{\sigma}\times\frac{h_0 r_0}{r_0 + ut\tan\theta}} \tag{B1}$$

$$\ell_n\left(\frac{\eta_b}{\eta_0}\right) = \int_0^{t_b} \beta_{\max}\, \mathrm{d}t \tag{B2}$$

All parameters except for $t$ are independent on the time variable and thus, Eq. (B3) is arranged after substituting Eq. (B1) into Eq. (B2):

$$\ell_n\left(\frac{\eta_b}{\eta_0}\right) = \frac{u^2}{2}\left(\frac{\rho_g}{\rho_l}\right)\sqrt{\frac{\rho_l}{\sigma h_0 r_0}}\times\int_0^{t_b}\sqrt{r_0 + ut\tan\theta}\,\mathrm{d}t \tag{B3}$$

After integrating Eq. (B3) and rearranging the integrated result, the breakup time $t_b$ is given by Eq. (B4). Here, $We_l$ is defined as $\rho_l u^2 h_0/\sigma$. The breakup length $z_b$ is derived by multiplying Eq. (B4) and axial velocity $u$. Finally, the corrected breakup length derived from linear instability theory is given as in Eq. (B5) by leaving only

the injection and ambient conditions in the right-hand side:

$$t_b = \frac{r_0}{u \tan\theta}\left[\left(C\frac{h_0 \tan\theta}{r_0}\left(\frac{\rho_g}{\rho_l}\right)^{-1} We_l^{-1/2} + 1\right)^{2/3} - 1\right] \quad \text{(B4)}$$

$$\left(\frac{r_0}{h_0 \tan\theta}\right)\left[\left(\frac{z_b \tan\theta}{r_0} + 1\right)^{3/2} - 1\right] = C(\rho_g/\rho_l)^{-1} We_l^{-1/2} \quad \text{(B5)}$$

## Acknowledgments

This research was supported by the Korea Space Launch Vehicle (KSLV)-I project and the National Research Laboratory Program (M1-0104-00-0058). The authors wish to acknowledge this financial support.

## References

[1] Lefebvre, A. H., *Gas Turbine Combustion*, Taylor & Francis, London, 1999.

[2] Lefebvre, A. H., *Atomization and Sprays*, Hemisphere, New York, 1989.

[3] Taylor, G. I., "The Boundary Layer in the Converging Nozzle of a Swirl Atomizer," *Quarterly Journal of Mechanics and Applied Mathematics*, Vol. 3, Pt. 2, 1950, pp. 129–139.

[4] Bayvel, L., and Orzechowski, Z., *Liquid Atomization*, Taylor & Francis, London, 1993.

[5] Rizk, N. K., and Lefebvre, A. H., "Internal Flow Characteristics of Simplex Swirl Atomizer," *Journal of Propulsion and Power*, Vol. 1, No. 3, 1985, pp. 193–199.

[6] De Corso, S. M., and Kemeny, G. A., "Effect of Ambient and Fuel Pressure on Nozzle Spray Angle," *ASME Transactions. Journal of Tribology*, Vol. 79, No. 3, 1957, pp. 607–615.

[7] Wang, X. F., and Lefebvre, A. H., "Influence of Ambient Air Pressure on Pressure-Swirl Atomization," *Atomisation and Spray Technology*, Vol. 3, No. 3, 1987, pp. 209–226.

[8] Dodge, L. G., and Biaglow, J. A., "Effect of Elevated Temperature and Pressure on Sprays from Simplex Swirl Atomizers," *Journal of Engineering for Gas Turbines and Power*, Vol. 108, No. 1, 1985, pp. 209–215; also Paper No. 85-GT-0058.

[9] Jasuja, A. K., and Lefebvre, A. H., "Influence of Ambient Air Pressure on Pressure-Swirl Atomizer Spray Characteristics," ASME Paper 2001-GT-0043, 2001.

[10] Koh, H., Kim, D., Shin, S., and Yoon, Y., "Spray Characterization in High Pressure Environment Using Optical Line Patternator," *Measurement Science and Technology*, Vol. 17, No. 8, 2006, pp. 2159–2167.

[11] Horvay, M., and Leuckel, W., "Experimental and Theoretical Investigation of Swirl Nozzles for Pressure-Jet Atomization," *German Chemical Engineering*, Vol. 9, No. 5, 1986, pp. 276–283.

[12] Lee, S. Y., and Tankin, R. S., "Study of Liquid Spray (Water) in a Non-Condensable Environment (Air)," *International Journal of Heat and Mass Transfer*, Vol. 27, No. 3, 1984, pp. 351–361.

[13] Rothe, P. H., and Block, J. A., "Aerodynamic Behavior of Liquid Sprays," *International Journal of Multiphase Flow*, Vol. 3, No. 3, 1977, pp. 263–272.

[14] Squire, H. B., "Investigation of the Instability of a Moving Liquid Film," *British Journal of Applied Physics*, Vol. 4, No. 6, 1953, pp. 167–169.

[15] Dombrowski, N., and Hooper, P. C., "The Effect of Ambient Density on Drop Formation in Sprays," *Chemical Engineering Science*, Vol. 17, No. 5, 1962, pp. 291–305.

[16] Hagerty, W. W., and Shea, J. F., "A Study of the Stability of Plane Fluid Sheets," *Journal of Applied Mechanics*, Vol. 22, No. 3, 1955, pp. 509–514.

[17] Panchagnula, M. V., Sojka, P. E., and Santangelo, P. J., "On the Three-Dimensional Instability of a Swirling, Annular, Inviscid Liquid Sheet Subject to Unequal Gas Velocities," *Physics of Fluids*, Vol. 8, No. 12, 1996, pp. 3300–3312.

[18] Ibrahim, A. A., Jog, M. A., and Jeng, S. M., "Effect of Liquid Swirl Velocity Profile on the Instability of a Swirling Annular Liquid Sheet," *Atomization and Sprays*, Vol. 16, No. 3, 2006, pp. 237–264.

[19] Borodin, V. A., Dityakin, Y. F., Klyachko, L. A., and Tagodkin, V. I., "Atomization of Liquids," Air Force Foreign Technology Division Rept., FTD-MT-24-97-68(AD685151), 1968.

T. Lieuwen
*Associate Editor*